Symmetric periodic orbits and global dynamics of tori in an O(2) equivariant system: Two-dimensional thermal convection

Marta Net[1]*and Juan Sánchez[1]

[1]Departament de Física Aplicada, Universitat Politècnica de
Catalunya Mòdul B4. Campus Nord 08034 Barcelona, Spain

January 31, 2006

Abstract

Numerical simulations of two-dimensional Boussinesq thermal convection in a long cylindrical annulus with radial gravity and heating are used to study the influence of the reflection and rotation symmetries of the system on the sequence of local and global bifurcations leading to complex time dependent behaviour. From the results of the linear stability analysis of symmetric periodic orbits, it is shown how, via gluing bifurcations, some quasi-periodic flows recover, as sets, symmetries lost in previous bifurcations. It is also shown how the same mechanism gives rise to a temporal chaotic attractor consisting of random switches between the symmetry-conjugate quasi-periodic orbits. At higher Rayleigh numbers, a chaotic-drifting behaviour is found when a circle of invariant tori loses stability. In addition, detailed information about the Floquet multipliers and eigenfuntions of the periodic orbits involved in this dynamics is supplied.

1   Introduction

Despite the free thermal convection is one of the classical problems in the Fluid Mechanics, it is difficult to find any paper detailing the transition between steady and quasi-periodic or chaotic stable solutions when they arise after bifurcations of unstable periodic flows. In

---

*Corresponding author: e-mail address marta@fa.upc.edu; Tel. 34-93-4017980; Fax 34-93-4016090

this paper we explain the origin of some stable quasi-periodic and temporal-chaotic flows found in [Net *et al.*, 2003], for a two-dimensional radial thermal convection problem of a low Prandtl number fluid in a long cylindrical annulus. In order to identify the sequence of bifurcations giving rise to these complex flows, we calculate and analyze the spectra of the unstable branches of periodic orbits from which they bifurcate.

For the range of parameter values studied, the periodic solutions are direction reversing travelling waves [Landsberg & Knobloch, 1991] (DRTWs), also known as pulsating waves [Proctor & Weiss, 1993]. They arise from a Hopf bifurcation on a circle of steady states, which breaks their reflection symmetry [Landsberg & Knobloch, 1991]. The solutions vacillate azimuthally, but have no net drift over the whole period of oscillation. However, it will be seen that subsequent bifurcations of the DRTWs lead to a wide variety of non-drifting and drifting quasi-periodic flows, including three-frequency states. The transition to turbulence through quasi-periodic states with three frequencies and the phase locking phenomenon in thermal convection was already detected in early laboratory experiments (see for instance [Maurer & Libchaber, 1979, 1980]).

The main objective of the paper is to explore in detail the dynamics and symmetries of the invariant tori, densely filled by modulated direction reversing travelling waves without net azimuthal drift (MDRTWs), to elucidate the mechanism that gives rise to chaotic switching between symmetry-conjugate solutions, and the influence of the $O(2)$ symmetry on the subsequent azimuthally drifting dynamics.

The annular convection at low Prandtl numbers ($\sigma = 0.025$ in our calculations) is the simplest model of equatorial convection in planetary interiors, but the results and the numerical techniques of analysis presented in the paper are also applicable to other problems equivariant under the same symmetry group. Such is the case of theynamics that arises on a thin smetic-A liquid crystal film suspended in a small annulus, with an electric field applied in the radial direction [Daya *et al.*, 1998], or in two-dimensional Rayleigh-Bénard convection in a periodic layer with broken mid plane symmetry, among others.

The bifurcations and patterns that may be observed in nature are independent of the source of instability (thermal, electrical, centrifugal, etc). They are determined qualitatively by mathematical properties, such as the geometry and the symmetries of the model. The physics of a problem selects through the parameters a particular pattern and the quantitative values of the variables. An important number of papers in different areas dealing with gluing bifurcations of periodic orbits have appeared, mainly in Z_2 equivariant systems. Numerical examples, in Rayleigh-Bénard convection [Massaguer *et al.*, 1990], magnetohydrodynamics [Rucklidge & Matthews, 1996], reaction-diffusion processes [Kuramoto & Koga, 1982], and even experimental examples in optothermal devices [Herrero *et al.*, 1998], or in electrohydrodynamic convection in a liquid crystal [Peacock & Mullin, 2001], among others, show transitions to preturbulent flows through gluing bifurcations of periodic orbits. It is more difficult to find in the literature an accurate description of this

dynamics for quasi-periodic solutions. Examples of this behaviour are found for a Kolmogorov flow in a system with D_4 symmetry [Armbruster *et al.*, 1996], or involving two and three-tori for a periodically-forced Taylor-Couette system with Z_2 symmetry [Lopez & Marques, 2000]. We show that, in systems with $O(2)$ symmetry, gluing bifurcations of tori may lead to a *figure-of-eight* temporal-chaotic attractor, i.e., that pairs of tori belonging to a continuous group orbit can behave as the attractors in systems with Z_2 or D_4 symmetries, because they remain reflection-invariant after a Neimark-Sacker bifurcation of symmetric periodic orbits.

The paper is organized as follows. After the introduction and the statement of the problem in Sec. 2, Sec. 3 is devoted to describe the bifurcation diagram of DRTWs. It seeks to clarify the origin of the invariant tori (MDRTWs). In Sec. 4 their dynamics is studied. Sec. 5 deals with the chaotic-drifting dynamics found far from the gluing bifurcations when the invariant tori lose stability. Finally, the paper concludes in Sec. 6 with a summary and discussion of the results. We also provide interested researchers with information about the spectra of the circles of DRTWs involved in this dynamics.

2 Basic equations

We consider an annular section of a cylindrical annulus of gap width $d \equiv r_o - r_i$, where r_i and r_o are the inner and outer radii, and radius ratio $\eta \equiv r_i/r_o = 0.3$. The inner and outer side contours are maintained at constant temperatures T_i and T_o respectively, with $T_i > T_o$, and for the velocity field no-slip lateral boundary conditions $u = v = 0$ on $r = r_i, r_o$ are taken. A constant gravity across the convective layer, $\mathbf{g} = -g\mathbf{e}_r$ is imposed.

The Boussinesq approximation of the two-dimensional Navier-Stokes, mass conservation and energy equations are written, in nondimensional form, by using as units the gap width, the temperature difference between the side boundaries, and the thermal diffusion time d^2/κ, where κ represents the thermal diffusivity. With the velocity field $\mathbf{u} = f\hat{\mathbf{e}}_\theta + \nabla \times (\psi\hat{\mathbf{e}}_z)$, the streamfunction formulation of the problem is

$$(\partial_t - \sigma\tilde{\Delta})f = P_\theta\Big[\Delta\psi(\frac{1}{r}\partial_\theta\psi)\Big], \tag{1}$$

$$(\partial_t - \sigma\Delta)\Delta\psi = \frac{\sigma Ra}{r}\partial_\theta\Theta + (1 - P_\theta)J(\psi, \Delta\psi) + \tilde{\Delta}f(\frac{1}{r}\partial_\theta\psi) - f(\frac{1}{r}\partial_\theta\Delta\psi), \tag{2}$$

$$(\partial_t - \Delta)\Theta = -\frac{1}{r^2\ln\eta}\partial_\theta\psi + J(\psi, \Theta) - f(\frac{1}{r}\partial_\theta\Theta), \tag{3}$$

and the boundary conditions are $f = \psi = \partial_r\psi = \Theta = 0$, on $r = r_i, r_o$.

The function $f(t, r)$ is needed to guarantee the possible existence of an azimuthal mean flow, if the azimuthal average of $\psi(t, r, \theta)$ is imposed to be zero by the homogeneous

3

boundary conditions. According this formulation, the streamfunction is

$$\Psi(t, r, \theta) = \psi(t, r, \theta) - \int_{r_i}^{r} f(t, r) \, dr,$$

and $\Theta = T - T_c$ means the perturbation of the conductive temperature T_c. P_θ is the operator that averages in the azimuthal direction, Δ is the horizontal Laplacian operator in polar coordinates, $J(g, h) = (\partial_r g \partial_\theta h - \partial_r h \partial_\theta g)/r$ and $\tilde{\Delta} = \partial_r(\partial_r + 1/r)$. The nondimensional parameters that appear in the equations are the Rayleigh and Prandtl numbers defined by

$$Ra \equiv \frac{\alpha \Delta T g d^3}{\kappa \nu}, \qquad \sigma \equiv \frac{\nu}{\kappa}.$$

For more information about the formulation of the problem see [Pino *et al.*, 2000].

The above system is $O(2)$ equivariant, i.e., equivariant under arbitrary azimuthal rotations R_α, and reflections by any diameter $\theta = \theta_0$, ζ_{θ_0}:

$$R_\alpha : \qquad (f, \psi, \Theta)(r, \theta) \to (f, \psi, \Theta)(r, \theta + \alpha)$$

$$\zeta_{\theta_0} : \qquad (f, \psi, \Theta)(r, \theta) \to (-f, -\psi, \Theta)(r, 2\theta_0 - \theta).$$

The equations are integrated numerically, mainly by using a fourth order semi-implicit BDF-extrapolation time-stepping code. The fields (f, ψ, Θ) are expanded in Chebyshev and Fourier polynomials in r and θ respectively. To study the dependence of the stable and unstable periodic solutions on the Rayleigh number, two different continuation codes have been written; one with respect to the physical parameter, and the other with respect to the arc-length of the curve of solutions [Sánchez *et al.*, 2004]. Notice that for this moderately large system of equations standard techniques for ODEs do not work. To be sure that the quasi-periodic and chaotic solutions are not spurious, they have been recalculated using a time-splitting code, written in terms of the velocity field, (u, v). In this formulation, a reflection symmetry means $(u, v, \Theta)(r, \theta) \to (u, -v, \Theta)(r, 2\theta_0 - \theta)$. The stability of the orbits is studied by computing their Floquet multipliers (FM) with an Arnoldi method or, if it is required due to the complexity of the spectrum, a more expensive subspace iteration method.

As we will describe the solutions in terms of symmetries we introduce now some relevant definitions. Two sets $\mathbb{S}$ (periodic orbits or tori in our case) are said to be τ-conjugate if they are related by a linear transformation τ. In our geometry, the relationship between the azimuthal Fourier coefficients, a_n and b_n, of rotation-conjugate (R_α-conjugate) solutions, when the rotation belongs to the group Z_4 generated by $R_{\pi/2}$, is $b_n = a_n \exp(inj\pi/2)$, $j = 0, 1, 2, 3$, and between a pair of reflection-conjugate solutions through a diameter $\theta = \theta_0$ (ζ_{θ_0}-conjugate), is $b_n = \bar{a}_n \exp(-2in\theta_0)$, where the bar means complex-conjugation. In this problem the phase θ_0 is determined by the initial conditions, since they select the azimuthal orientation of the patterns. A set $\mathbb{S}$ is said to be τ-invariant if $\tau(\mathbb{S}) = \mathbb{S}$.

4

3   Time periodic solutions

In this section we identify the sequence of local bifurcations of symmetric periodic orbits leading to the MDRTWs of Sec. 4 for $Ra > 18440$.

The time dependence for the $R_{\pi/2}$-invariant solutions (from now on, pure $n = 4$ solutions) comes from a Hopf bifurcation of period $T_1 = 0.18$, at $Ra = 6897$ [Net *et al.*, 2003]. The bifurcation breaks the reflection symmetries, ζ_{θ_k}, of the steady solutions with respect to the diameters $\theta_k = \theta_0 + k\pi/4$, with $k = 0, 1, 2, 3$. However, the periodic orbits are symmetric, and in addition to the rotational symmetries, $R_{k\pi/2}$,

$$(f, \psi, \Theta)(t, r, \theta) = (f, \psi, \Theta)(t, r, \theta + k\pi/2),$$

they have the spatio-temporal symmetries

$$(f, \psi, \Theta)(t, r, \theta) = (-f, -\psi, \Theta)(t + T/2, r, 2\theta_k - \theta).$$

Their spatial symmetry group is Z_4, but it is D_4 if the spatio-temporal symmetries are considered. These orbits have an instantaneous mean azimuthal flow, $f(t, r)$, which vanishes when it is averaged in a whole temporal period.

The bifurcation diagram of Fig. 1 shows the branches of periodic orbits born from the pure $n = 4$ DRTWs for a fixed azimuthal phase. Some of the growing modes remain very small, therefore a weighted amplitude $A = \sum_{n=0}^{4} W_n |\Theta_n(r_p)|$, of the first five azimuthal Fourier coefficients, at the time at which the net mass flow

$$\overline{f}(t) = \frac{1}{r_o - r_i} \int_{r_i}^{r_o} f(t, r)\, dr$$

vanishes, is plotted. In the definition of A, r_p means a fixed radial point, and the weights, W_n, are selected to clearly distinguish the different branches. The stability of these solutions is also analyzed. The number of FM outside the unit circle is indicated beside each branch. In addition, the spectrum of every solution has a marginal real $\mu = 1$ FM because of the rotational invariance of the system. The associated eigenfunction is $(0, \partial_\theta \psi, \partial_\theta \Theta)$ (see Fig. 2(a, b)).

At $Ra = 10210$ the pure $n = 4$ DRTWs lose stability in a subharmonic pitchfork bifurcation of periodic orbits. The new branches are $R_{\pi/2}$-conjugate. The bifurcated solutions (from now on, pure $n = 2$ DRTWs) are R_π-invariant, and maintain two spatio-temporal symmetries. The change of symmetry can be observed in the snapshots of Fig. 3(a-h) (see figure caption for their meaning). On the pure $n = 2$ branch the four identical pairs of vortices of the $n = 4$ branch become two couples of identical pairs of vortices.

At $Ra = 10430$, the $n = 2$ DRTWs lose stability in a second pitchfork bifurcation that breaks the R_π-symmetry by the growth of the azimuthal odd wave numbers, but

5

keeps a spatio-temporal symmetry. Now, the branches born at the bifurcation point are R_π-conjugate (see Fig. 4(a-e)). For these solutions all the pairs of vortices are different.

A second pitchfork bifurcation on the already unstable $n = 2$ branch of DRTWs takes places at $Ra = 10784.9$. The critical eigenfunction is shown in Fig. 5(a, b). On the new branch of DRTWs, there is a Neimark-Sacker transition at $Ra = 10790.6$, (marked with an asterisk in Fig. 1 and Fig. 6(a)) of very small imaginary part. To confirm that the latter bifurcation cannot generate the dynamics of Sec. 4, we have estimated the second critical frequency, computed from the critical complex FM $\mu_{1,2} = 0.99995 \pm 0.01224i$, and the main frequency $f_1 = 6.922$ of the periodic orbit at the bifurcation point. It gives $f_2{}^c = 0.0135$, which is almost two orders of magnitude lesser than the frequency $f_2 = 0.83$ of the stable MDTRWs found at $Ra = 18500$.

The behaviour of the dominant $|\mu| < 1$ FM near $Ra = 10784.9$ is sketched in Fig. 6(a-c), because it also provides the mechanism giving rise to the three-torus described in the next two paragraphs. On the $n = 2$ branch at $Ra = 10783.1$ (empty circle (1) of Fig. 6(a)) two complex-conjugate FM of diminishing frequency become real at $\mu = 0.994$. By increasing Ra one of them grows, and crosses the unit circle, while the other moves back (Fig. 6(b)). The complex-conjugate pair crossing the unit circle, comes from the collision at $\mu = 0.996$ (empty circle (2) of Fig. 6(a)) of the real FM responsible of the previous bifurcation, which was moving back along this branch, with another real FM, which was growing (Fig. 6(c)). By slightly moving the radius ratio the pitchfork and the Neimark-Sacker bifurcations would collapse in a triple $+1$ bifurcation.

The stable DRTWs, born at $Ra = 10430$, soon undergo a new bifurcation, marked with a cross in Fig. 1, at $Ra = 11401.0$. This is the only real bifurcation that breaks all the spatio-temporal symmetries. Near the transition, the dominant eigenvalues behave again in the way described in the above paragraph; i.e., before the bifurcation, the imaginary part of two complex-conjugate FM vanishes at $Ra = 11399.1$ with $\mu = 0.996$, and only one of them becomes unstable. We have observed that its corresponding eigenvector tends to the azimuthal derivative of the function as it approaches the bifurcation point. In consequence the Jordan block corresponding to the double $+1$ FM will be of order two, and azimuthal drifting dynamics must be expected. The existence of drifting DRTWs is in agreement with previous results that prove that a real bifurcation from a circle of symmetric orbits can lead to drifting solutions [Rucklidge & Silver, 1998; Lamb & Melbourne, 1999; Lamb et al., 2003] (see also references therein).

By increasing the parameter value, instead of a drifting DRTW, the time evolution codes detect a stable three-frequency regime ($\mathbb{T}^3$) consisting of a modulated drifting DRTW, i.e., they detect the expected rotating wave, but with an additional frequency. The presence of this complex solution so close to the bifurcation point is due to the proximity to a non-generic triple $+1$ bifurcation, i.e., the diagram of Fig. 6(a) also represents the behaviour of the FM near the point marked with the cross. In this case, the first bifurcation (cross) gives rise to the drift of the DRTW, and the second (now of a torus)

to its modulation. The drifting DRTW only exists in a very narrow region between two bifurcations.

The Fourier spectrum of the $n = 4$ azimuthal Fourier coefficient of one of the orbits on the $\mathbb{T}^3$ at $Ra = 11430$ is displayed in Fig. 7(a, b). The very small frequency $f_2 = 1.91 \times 10^{-4}$ is the drifting frequency and $f_3 = 1.41 \times 10^{-2}$ is the modulation frequency, which produces a back and forth drift in the azimuthal direction. The highest frequency $f_1 = 7.10$ corresponds to the azimuthal initial vacillation of the DRTWs. With an annulus of gap width $d = 25$ cm, the very low frequency, f_2, represents that it would take 35 days for a vortex to complete a turn around the annulus. When Ra is moved away from the bifurcation point, f_2 increases, although this frequency is locked in some intervals of the parameter space, and MDRTWs arise. However, its modulation frequency f_3 is again almost two orders of magnitude lesser than 0.83. In addition, the modulated drifting waves are lost near $Ra = 11590$.

At $Ra = 17497$, the $n = 2$ branch of DRTWs presents a new slightly subcritical pitchfork bifurcation. The contour plots showing the loss of symmetry of the solutions on the new R_π-conjugate branches (labeled $n = 1$ in Fig. 1) can be seen in Fig. 8(a-e).

Following the $n = 1$ branch, at $Ra = 18682$, a pair of complex-conjugate FM crosses the unit circle generating a branch of unstable quasi-periodic solutions, which, at higher parameter values, gives rise to the global dynamics presented in Sec. 4. Stable MDRTWs are found below the bifurcation point down to $Ra \approx 18440$, with the time evolution codes. We have compared the estimate of the second critical frequency $f_2{}^c = 0.88$, computed, as before, from the critical FM, $\mu_{1,2} = 0.837 \pm 0.547i$, and the main frequency $f_1 = 9.60$ of the periodic orbit at the bifurcation point, with the frequency $f_2 = 0.83$ of the stable quasi-periodic orbit at $Ra = 18500$. Both frequencies are close enough to indicate that this stable branch of tori is connected with the periodic orbits through the bifurcation at $Ra = 18682$, which should be subcritical. To know exactly how the tori stabilize it would be necessary to calculate unstable tori and their transversal stability.

To understand the global behaviour of Sec. 4 we include in this section the results of the linear stability analysis of the pure $n = 4$ DRTWs. They show that there are two other bifurcation points on this branch. At the first, which takes place at $Ra = 14660$, a double real FM crosses the unit circle. It is straightforward to show that, since $R_{\pi/2}$ commutes with the differential of the Poincaré map, and the eigenfunction of Fig. 9(a, b) breaks all the spatial rotation symmetries, by applying $R_{\pi/2}$ a linearly independent eigenfunction (Fig. 9(c, d)) is obtained. In consequence, the critical $\mu = +1$ FM is generically forced to have multiplicity two. These marginal modes keep a spatio-temporal symmetry, therefore the new periodic orbits are DRTWs without spatial symmetries. The following bifurcation on the $n = 4$ curve of solutions takes place at $Ra = 15866$, when the FM, which becomes unstable at $Ra = 10210$, and remains close to the unit circle, moves back. From this point, and at least up to $Ra = 27000$, there are not other bifurcations on the $n = 4$ branch.

It will be shown that only the pure $n = 4$ and the $n = 1$ branches are involved in the

7

dynamics of the MDRTWs found for $Ra > 18440$. The leading FM in this range of Ra can be seen in Tables 1 and 2, respectively.

4   Invariant tori: Symmetry properties and gluing bifurcations

The scheme of Fig. 10 illustrates the sequence of direct and inverse period-doubling (PD), saddle-node (SN), and gluing (GL) bifurcations leading to temporal chaotic attractors (CH). It is based on the transients we have observed, and on the invariances of the tori of Fig. 11(a,b) and Fig. 12. In these projections of the Poincaré sections, odd azimuthal Fourier coefficients of the components of the velocity field are plotted. Thus, the unstable pure $n = 4$ periodic solution is at the origin, and a R_π-rotation can be directly observed in the plots.

For $Ra > 18440$ ($SN1$), stable branches of tori bifurcated from the R_π-conjugate $n = 1$ branches of DRTWs at $Ra = 18682$ are found. Fig. 11(c) shows the time evolution of the phase of four Fourier coefficients, a_n and b_n, of a trajectory on each tori of Fig. 11(a) at $Ra = 20000$, after a time shift. Since $f_2 \ll f_1$, the figure shows very clearly that the tori are related by R_π, i.e., that $b_n = a_n \exp(in\pi)$.

Fig. 11(d) displays the sum of the phases of same n in Fig. 11(c) versus time. They are almost constant and equal to $-2n\theta_0$, with $\theta_0 = -\pi/4$ determined by the initial conditions. Then $b_n = \bar{a}_n \exp(in\pi/2)$, and the tori are also $\zeta_{-\pi/4}$-conjugate. This is so because they come from pairs of R_π-conjugate DRTWs, and each torus is $\zeta_{\pi/4}$-invariant. The Neimark-Sacker bifurcation takes place from solutions that do not retain any spatial symmetry, but are symmetric periodic orbits. In addition, the solutions do not drift along their group orbit. So, it seems that the bifurcation theory for transitions from isolated S-cycles [Kuznetsov, 1998] applies, and the emerging tori must be invariant under the reflection that define the symmetric periodic orbit; for the initial condition of this case $\zeta_{\pi/4}$.

The $\zeta_{\pi/4}$-invariance of the tori allow them to be, at the same time, $\zeta_{-\pi/4}$-conjugate and R_π-conjugate. In effect, if $\mathbb{T}_1$ and $\mathbb{T}_2$ are two rotation-conjugate tori, $R_{\theta_1}(\mathbb{T}_1) = \mathbb{T}_2$, and, in addition, $\mathbb{T}_1$ is reflection-invariant, $\zeta_{\theta_2}(\mathbb{T}_1) = \mathbb{T}_1$, then $R_{\theta_1}\zeta_{\theta_2}(\mathbb{T}_1) = \mathbb{T}_2$. On the other hand, $R_{\theta_1}\zeta_{\theta_2} = \zeta_{\theta_3}$ with $\theta_3 = (\theta_1 + 2\theta_2)/2$, so they are ζ_{θ_3}-conjugate, $\zeta_{\theta_3}(\mathbb{T}_1) = \mathbb{T}_2$. This result agree with our calculations. With an initial condition that gives $\theta_2 = \pi/4$ and $\theta_1 = \pi$, $\theta_3 = -\pi/4$.

To find the symmetries of a torus we have plotted the distance

$$d = \min_t \parallel x(t, r_p) - \tau_\theta x(0, r_p) \parallel_2,$$

for a very long time sequence of a quasi-periodic orbit on the torus versus the angle of transformation. In the definition of the d, $x(t, r_p) = (f(t, r_p), \Re\psi_1(t, r_p), \Im\psi_1(t, r_p), ..., \Im\psi_4(t, r_p))$,

8

τ_θ means either a rotation or a reflection, and r_p a fixed radial point. Fig. 13(a,b) displays this distance d for a tori of Fig. 11(a), and the torus of Fig. 12(e), respectively. Red lines refer to rotations (from 0 to 2π) and blue lines to reflections (from 0 to π). It is clear from Fig. 13(a) that $d \ll 1$ only for $\zeta_{\pi/4}$, while in Fig. 13(b) $d \ll 1$ for $\zeta_{\pi/4}$, $\zeta_{-\pi/4}$ and R_π. The distance d depends on the length of the trajectory considered. From now on, we will call small (big) tori to those that are invariant under a reflection (two reflections and a π rotation).

The long period T_2 of the quasi-periodic orbits and its maximum amplitude increase with Ra until $Ra \approx 20000$, where they seem to saturate. At $Ra \approx 20160$ ($PD1$) the period T_2 doubles (see Fig. 11(b)), and at $Ra \approx 20170$, the new tori lose stability in a saddle-node bifurcation of tori ($SN2$). The transients show that, along the unstable branch ($SN2$ to $GL1$), the internal loops of the pair of period-doubled small tori approach the $n = 1$ periodic orbits from which they bifurcate. Simultaneously the external loops become homoclinic to the origin with the standard return direction (see [Kuznetsov, 1998]), giving rise to a stable temporal-chaotic flow in $GL1$.

The new solutions, which are represented in Fig. 12(a), remain nearly homoclinic to the $n = 4$ DRTW forming a *figure-of-eight* chaotic attractor. When the trajectories approach the origin, the $n \neq 4$ amplitudes tend to zero (see also Fig. 10 in [Net *et al.*, 2003]). Then it is clear that the director center of the quasi-periodic dynamics, presented below, is the $n = 4$ DRTW. Long time sequences of these solutions and their Fourier spectra (see Fig. 14(a, b)) reveal that the non-periodic behaviour consists of random switches between conjugated tori. By increasing the control parameter following the branch CH, the Poincaré sections vary continuously diminishing its randomness and becoming nearly periodic, of long period $8T_2$ (Fig. 12(b,c)). These solutions disappear in another gluing bifurcation involving hysteresis (point $GL2$).

In order to understand the connection between the chaotic behaviour and the quasi-periodic dynamics found beyond $GL2$, it is easier to examine the sequence of bifurcations from CB to $GL2$. By decreasing Ra from CB, the big torus of Fig. 12(j) becomes homoclinic to the $n = 4$ DRTW near $Ra = 21010$ ($GL4$), forming a *figure-of-eight* Poincaré section, approximated in Fig. 12(i). The long period of the quasi-periodic solutions has the monotone dependence on the parameter characteristic of the saddle homoclinic bifurcations, tending to infinity at the bifurcation point.

We have seen that the big tori have a triple invariance as sets, i.e., they are $\zeta_{\pi/4}$, $\zeta_{-\pi/4}$ and R_π-invariant. This happens because in the increasing direction of the parameter $GL4$ is a gluing bifurcation of a pair of $\zeta_{-\pi/4}$-conjugate and R_π-conjugate small tori (Fig. 12(h)), which are $\zeta_{\pi/4}$-invariant. In consequence, the resulting big torus has to be invariant under $\zeta_{-\pi/4}$ and R_π. In addition, $R_\pi \zeta_{-\pi/4} = \zeta_{\pi/4}$, so is also $\zeta_{\pi/4}$-invariant.

By decreasing Ra further, the small tori double their long period in $PD2$ (Fig. 12(g)). Subsequently, very close to the period-doubling bifurcation, the new pair of tori of long period near $2T_2$, glue in $GL3$ at $Ra \approx 20885$, giving rise to the single big double-lobed

9

tori of Fig. 12(f). As in the preceding case, by moving away from the critical parameter, the long period starts to decrease from infinity in a monotone way to approximately $4T_2$. The denser number of points near the origin in the Poincaré sections indicates that, very close to the gluing bifurcation point, the trajectories of the quasi-periodic solutions spend long times near the pure $n = 4$ DRTW, before escaping following its unstable manifold and turning around the unstable $n = 1$ DRTWs placed inside the loops.

By decreasing Ra even more, the trajectories separate from the origin, while the internal loops contract, approaching the internal periodic orbits (Fig. 12(e)). This big torus remains stable down to $Ra \approx 20211$, where it loses stability in a subcritical pitchfork bifurcation of tori (PF). The branch going from PF to $GL2$ is unstable, but the shape of the Poincaré section of the new solutions can be guessed from the transient of Fig. 12(d). It is obtained by perturbing the big stable torus in the region where symmetric and asymmetric big tori coexist.

The shape of the asymmetric big tori and the inverse gluing bifurcation $GL2$ are sketched in Fig. 15. It is a gluing bifurcation in the non-standard return direction (see [Kuznetsov, 1998]). The new solution of long period $8T_2$ is very similar to the chaotic solution shown in Fig. 12(c), but it must be pointed out that we have been unable to capture a pure two-lobed torus with four loops on each side. Instead of a new period-doubled solution, the chaotic attractor is found. The numerical results do not allow to asses whether this happens because the random switches between reflection-conjugate orbits start at this gluing connection, or simply because the torus is stable in a narrow range very near the gluing point. However, the temporal series of solutions of the chaotic branch, like that of Fig. 14(a), which show that sequences with more than four loops around the $n = 1$ DRTWs do not exist, and even some experimental results [von Stamm *et al.*, 1996], support the first hypothesis.

5   Chaotic-drifting behaviour

Due to the invariance of the system by arbitrary rotations, any of the solutions in Fig. 12 has an uncountable number of other R_α-conjugate solutions that only differ in the azimuthal orientation of the vortices; so, with arbitrary initial conditions, the solutions we found are rotated in an arbitrary azimuthal phase.

At $Ra = 22330 \pm 0.15\%$, the big tori lose stability, and, from CB, a global chaotic-drifting behaviour is found. Due to the existence of the group orbit, the trajectories consist of transient excursions among the R_α-conjugate unstable tori. Finally, in the range of parameters and initial conditions explored, they evolve to fast excursions among R_α-conjugate chaotic sets of main azimuthal wave number $n = 3$ ([Net *et al.*, 2003]).

Fig. 16 and 17 display two solutions at different Rayleigh numbers, starting with the same initial condition. Near the bifurcation point, the trajectory spends a long time in

the proximity of the torus before approaching another torus of the same group orbit, and, finally, the $n = 3$ branch. In this range of parameters it is easy to check the R_α-conjugation by computing the amplitude and phase of the bits of the temporal sequences of Fig. 16(a, b) that correspond to the same torus, as we have done for the stable conjugate tori of Fig. 11. Here the difference between the mean phases would give the angle rotated along the group orbit of big tori. However, the trajectories are extremely dependent on the initial conditions.

By increasing Ra further, less time is spent near each torus, but a longer time travelling among them. Fig. 17 is plotted at $Ra = 27000$ far from the point CB. It shows that after a shorter permanence near the initial tori, the solution starts quick excursions, visiting many tori randomly. By weakly perturbing the initial condition the qualitative dynamics remains unperturbed. The R_α-conjugate tori can be seen as small tears in Fig. 17(c) (enlargement of Fig. 17(b)), and as blue spots in the tridimensional phase map of Fig. 17(d). In this plot the XY plane contains the real and imaginary parts of the $n = 4$ azimuthal Fourier coefficient, so the red circle represents the group orbit of the $n = 4$ DRTW contained in $v(Re(n = 1)) = 0$. The chaotic orbits drift following this circle. The amplitude of the large oscillations of Fig. 17(c) is also independent of the initial conditions. The period of these oscillations gives an idea of the time it takes the system to go around the group orbit when the trajectory spends short times near every torus. From this long period it is possible to estimate a third frequency for the orbit, and consider it a perturbation of a three-frequency quasi-periodic solution.

It is not possible to know, only by means of direct simulations, if for larger Ra the system could stabilize in a solution consistent in permanent excursions among the R_α-conjugate tori. For the highest parameters explored ($Ra = 27000$) we have found fast excursions lasting more than 600 thermal time units. For mercury, this means four days in a small annular domain of gap width $d = 5$ cm.

6 Discussion and conclusions

Fig. 1 contain some interesting results that deserve to be emphasized. The stability analysis of the symmetric periodic orbits reveals that the spatial symmetries of the orbits seems to prevent the existence of bifurcations to travelling solutions. After the loss of all the spatial symmetries, an extra marginal $\mu = +1$ FM leads to drifting solutions. This type of bifurcation is generic from a circle of DRTWs (cross in the bifurcation diagram). From this point, we have found modulated rotating DRTWs because of the proximity to a non-generic triple +1 bifurcation. In addition, it is important to notice that on the branch of Z_4 spatial symmetric orbits the double +1 bifurcation is also generic. By moving the radius ratio, between $\eta = 0.3$ and $\eta = 0.35$, the subharmonic and the double +1 real bifurcations overlap in a non-generic triple +1 bifurcation (or quadruple if the $\mu = +1$

11

FM due to the rotation invariance is taken into account).

The disappearance of the pure $n = 2$ periodic orbits before the tori appear causes that only the $n = 4$ branch of DRTW and the $n = 1$ branch, from which the tori bifurcate, contribute to the quasi-periodic dynamics at high Ra values. The periodic orbits are the fixed points of the return-maps involved in the homoclinic connections.

We have found *laminar* ($GL3, GL4$) and *chaotic* gluing bifurcations ($GL1, GL2$). The behaviour of the system at these points is in part determined by the FM of the $n = 4$ and $n = 1$ DRTWs. Table 1 contains the five dominant FM of the spectra of the former. From $Ra = 15866$ only a double real FM maintains its modulus $\mu_{1,2} \approx +1.04$ almost constant and bigger than one, the next being also real. This means that the spectrum of one of the organizing centers of all the gluing bifurcations found is simply of saddle type, with a two-dimensional unstable manifold. The absence of curvature of the stable and unstable directions of the chaotic attractor of Fig. 12(a) near the origin confirms that the origin behaves as a saddle-node.

The spectra of Table 2 corresponds to the $n = 1$ DRTWs. From the bifurcation point ($Ra = 18682$), the spectra have a real and two complex-conjugate FM with $|\mu| > 1$. Their moduli approach and cross at $Ra \approx 20173$, where it is found that the quasi-periodic dynamics is lost, and the temporal chaotic attractor becomes apparent. In addition, during the chaotic behaviour (CH) they maintain their moduli almost fixed to $|\mu_{1,2,3}| \approx 1.072$. By increasing Ra further, the complex FM increase their moduli, moving away from the unit circle, while the real one approaches it. In this numerical work, it is impossible to state whether the three-dimensional unstable manifold of the $n = 1$ DRTWs with repelling directions of the same strength is a necessary condition for the existence of chaotic attractors from $GL1$ to $GL2$. In any case, we have supplied detailed information about the spectra of the DRTWs involved in the gluing bifurcations. It can be useful to bifurcation theory researchers in order to build reduced models with the same behaviour.

The global dynamics described in Sec. 5 has many common features with that described in [Armbruster *et al.*, 1996], in the sense that the saddle sets visited during the excursions are related by the symmetries of the system, and consequently the amplitude of the excursions is small compared with those of large amplitude bursting dynamics [Moehlis & Knobloch, 1998]. However, in our case, the system is $O(2)$ equivariant and the group orbit is continuous. To the present, it is almost impossible to calculate unstable quasi-periodic solutions by continuation methods, and neither their unstable manifolds in moderately high-dimensional systems. However, the chaotic-drifting behaviour appears after a change of stability of the big tori. This change drives the dynamics along the circle of orbits. The subsequent global dynamics could be reflected in the spectra of the periodic orbits. We have checked that the $|\mu| < 1$ third and fourth FM of the $n = 4$ DRTW cross at $Ra \approx 21750$ (see Table 1) and that, from this point, the eigenfunction corresponding to the dominant stable direction resembles very much the azimuthal derivative. This means that it has a large component tangent to the circle of periodic orbits. So, it seems that

when a chaotic orbit moves away from a torus and approaches the $n = 4$ periodic orbit, the azimuthal phase changes randomly, and a new torus of the group orbit is visited.

References

Armbruster, D., Nicolaenko, B., Smaoui, N. & Chossat, P. [1996] "Symmetries and dynamics for 2-D Navier-Stokes flow," *Physica D* **95**, 81–93.

Daya, Z. A., Deyirmenjian, V., Morris, S. & de Bruyn, J. R. [1998] "Annular electroconvection with shear," *Phys. Rev. Lett.* **80**(5), 964–967.

Herrero, R., Farjas, J., Pons, R., Pi, F. & Orriols, G. [1998] "Gluing bifurcations in optothermal nonlinear devices," *Phys. Rev. E* **57**(5), 5366–5377.

Kuramoto, Y. & Koga, S. [1982] "Anomalous period-doubling bifurcations leading to chemical turbulence," *Phys. Lett. A* **92**, 1–4.

Kuznetsov, Y. A. [1998] *Elements of Applied Bifurcation Theory, Second Edition*. Springer.

Lamb, J. S. W. & Melbourne, I. [1999] "Bifurcation from periodic solutions with spatiotemporal symmetry," in *Pattern formation in continuous and coupled systems*, eds. M. Golubitsky, D. Luss, & S. H. Strogatz. (Springer) volume 115 of *IMA*, pp. 175–191.

Lamb, J. S. W., Melbourne, I. & Wulff, C. [2003] "Bifurcation from periodic solutions with spatiotemporal symmetry, including resonances and mode interactions," *J. Differential Equations* **191**, 377–407.

Landsberg, A. S. & Knobloch, E. [1991] "Direction-reversing travelling waves," *Phys. Lett. A* **159**, 17–20.

Lopez, J. M. & Marques, F. [2000] "Dynamics of three-tori in a periodically forced Navier-Stokes flow," *Phys. Rev. Lett.* **85**(5), 972–975.

Massaguer, J., Mercader, I. & Net, M. [1990] "Nonlinear dynamics of vertical vorticity in low-Prandtl-number thermal convection," *J. Fluid Mech.* **214**, 579–597.

Maurer, J. & Libchaber, A. [1979] "Rayleigh-Bénard experiment in liquid helium; frequency locking and the onset of turbulence," *J. Phys. Lett.* **40**, 419–423.

Maurer, J. & Libchaber, A. [1980] "Effect of the Prandtl number on the onset of the turbulence in liquid ^4He," *J. Phys. Lett.* **41**, 515–518.

Moehlis, J. & Knobloch, E. [1998] "Forced symmetry breaking as a mechanism for bursting," *Phys. Rev. Lett.* **80**(24), 5329–5332.

Net, M., Alonso, A. & Sánchez, J. [2003] "From stationary to complex time-dependent flows in two-dimensional annular thermal convection at moderate Rayleigh numbers," *Phys. Fluids* **15**(5), 1314–1326.

Peacock, T. & Mullin, T. [2001] "Homoclinic bifurcations in a liquid crystal flow," *J. Fluid Mech.* **432**, 369–386.

Pino, D., Mercader, I. & Net, M. [2000] "Thermal and inertial modes of convection in a rapidly rotating annulus," *Phys. Rev. E* **61**(2), 1507–1517.

Proctor, M. R. E. & Weiss, N. O. [1993] "Symmetries of time-dependent magnetoconvenction," *Geophys. Astrophys. Fluid Dynamics* **70**, 137–160.

Rucklidge, A. M. & Matthews, P. C. [1996] "Analysis of the shearing instability in nonlinear convection and magnetoconvection," *Nonlinearity* **9**, 311–351.

Rucklidge, A. M. & Silver, M. [1998] "Bifurcations of periodic orbits with spatio-temporal symmetries," *Nonlinearity* **11**, 1435–1455.

Sánchez, J., Net, M., García-Archilla, B. & Simó, C. [2004] "Newton-Krylov continuation of periodic orbits for Navier-Stokes flows," *J. Comput. Phys.* **201**(1), 13–33.

von Stamm, J., Gerdts, U., Buzug, T. & Pfister, G. [1996] "Symmetry breaking and period doubling on a torus in the VLF regime in Taylor-Couette flow," *Phys. Rev. E* **54**(5), 4938–4957.
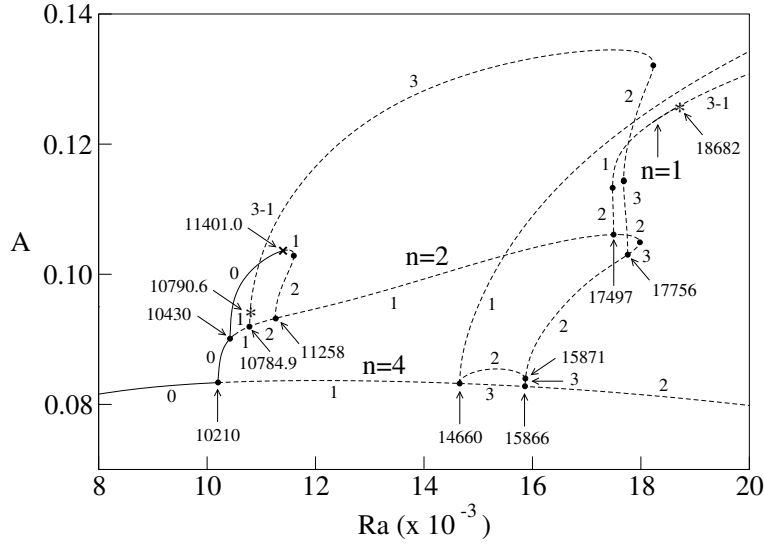
Figure 1: Bifurcation diagram of periodic orbits (DRTWs). An amplitude A (see text) versus the Rayleigh number is plotted. Solid and dashed lines mean stable and unstable solutions, respectively. The labels beside the branches indicate the total number of FM outside the unit circle. When there are complex pairs, the second number indicates how many FM are real.
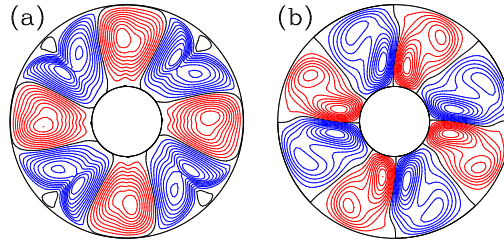

Figure 2: Contour plots of (a) the streamfunction Ψ, and (b) the temperature perturbation Θ of the eigenfunction of the $\mu = 1$ FM due to the invariance of the system by arbitrary rotations. Pure $n = 4$ DRTW at $Ra = 14660$.

15
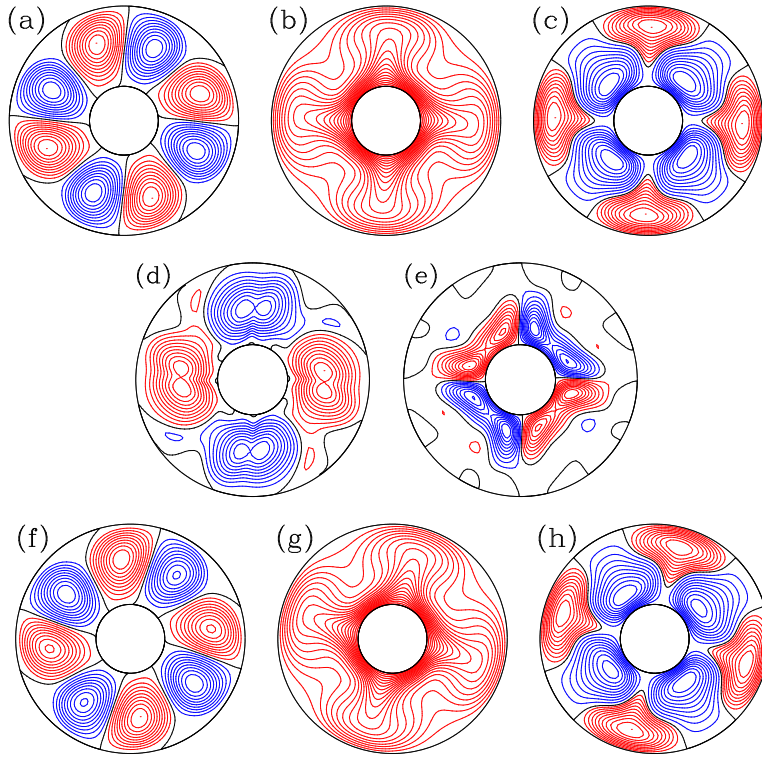
Figure 3: Contour plots of Ψ, T, and Θ. (a, b, c) for the stable pure $n = 4$ DRTW at $Ra = 10200$, and (f, g, h) for the stable subharmonic DRTW at $Ra = 10225$. (d, e) are, respectively, those of Ψ, and Θ for the eigenfunction of critical $\mu = 1$ FM at $Ra = 10210$.
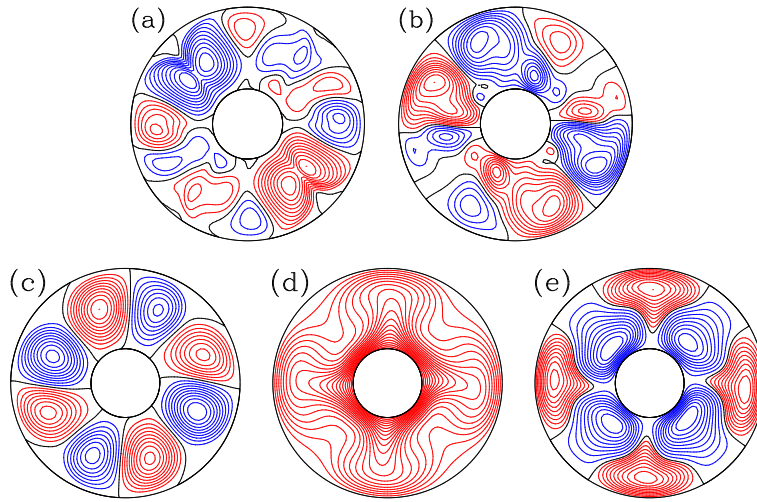
Figure 4: Contour plots of (a) Ψ, and (b) Θ of the eigenfunction of critical $\mu = 1$ FM at $Ra = 10430$. (c, d, e) are, respectively, those of the Ψ, T, and Θ for the new DRTW at $Ra = 10590$.
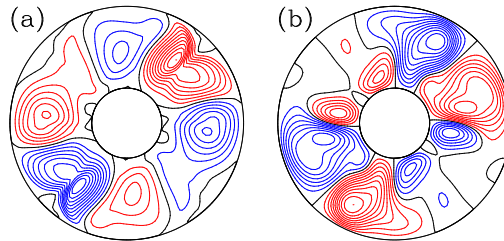
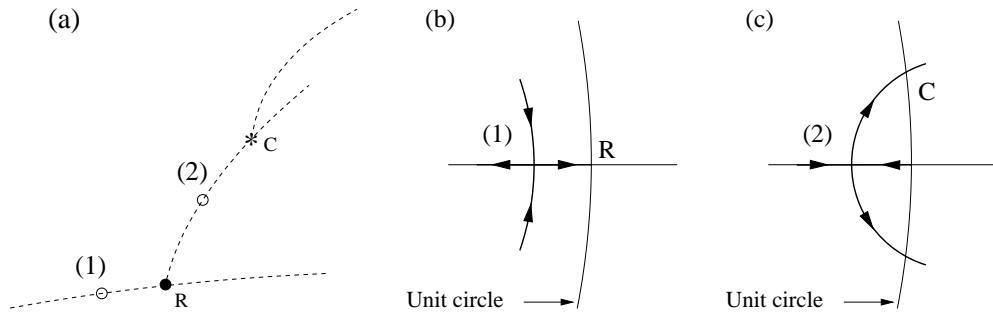Figure 5: Contour plots of (a) Ψ, and (b) Θ of the eigenfunction of critical $\mu = 1$ FM at $Ra = 10784.9$.

Figure 6: (a) Sketch of the bifurcation diagram near the points $Ra = 10784.9$ and $Ra = 11401.0$ of Fig. 2. The close circle (R) and the asterisk (C) indicate real $\mu = 1$ and complex bifurcations, respectively. The empty circles denote the points of collision of the FM. (b, c) Behaviour of the FM close to these bifurcations; (b) and (c) correspond to the collisions at points (1) and (2) of (a), respectively.
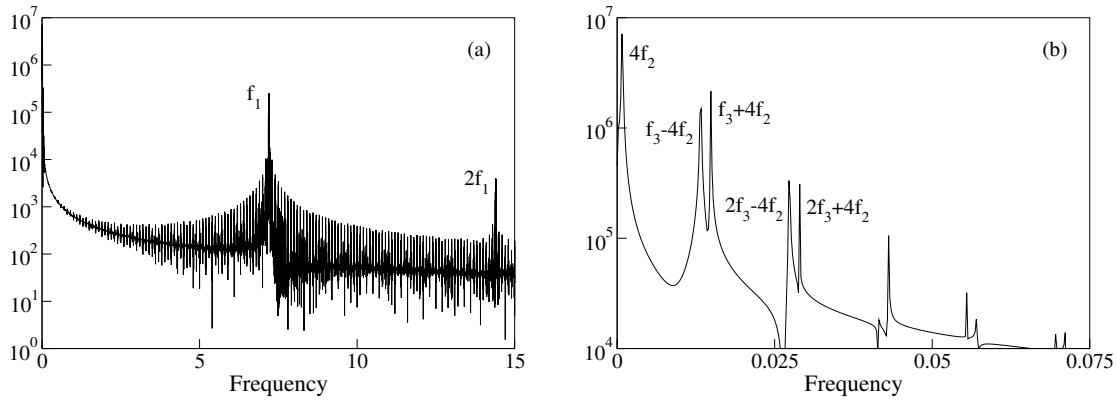

Figure 7: (a) Fourier spectrum of the modulated drifting DRTW found for $Ra \gtrsim 11401.0$, and (b) detail of (a) near the origin showing the low frequencies.
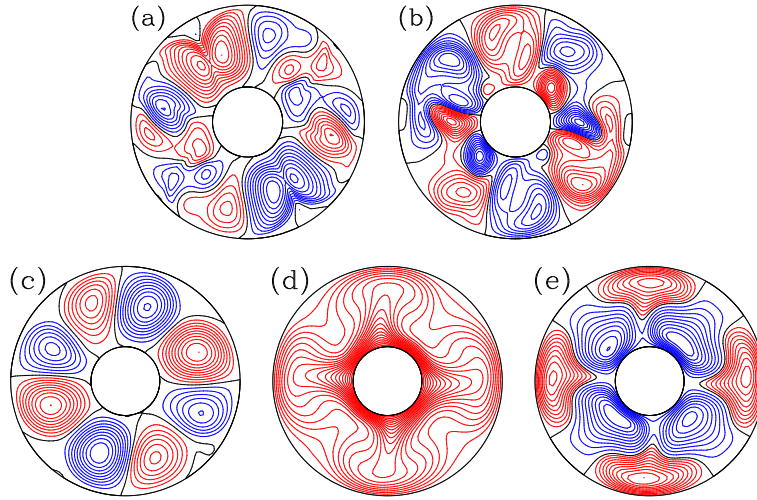
18

Figure 8: Contour plots of (a) Ψ, and (b) Θ of the eigenfunction of critical $\mu = 1$ FM at $Ra = 17497$. (c, d, e) are, respectively, those of Ψ, T, and Θ for the $n = 1$ DRTW at $Ra = 17800$.
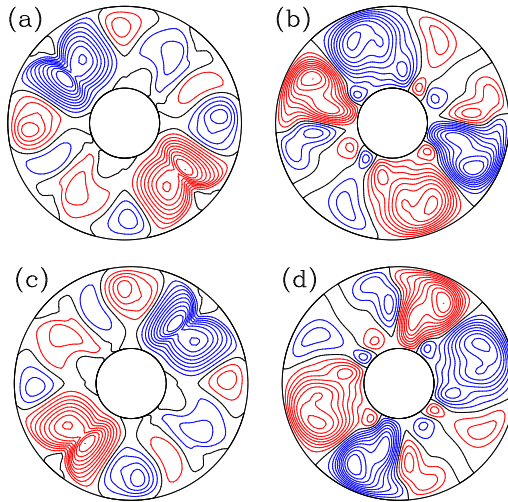

Figure 9: Contour plots of (a, c) Ψ, and (b, d) Θ of the eigenfunctions of the critical double $\mu = 1$ FM at $Ra = 14660$.
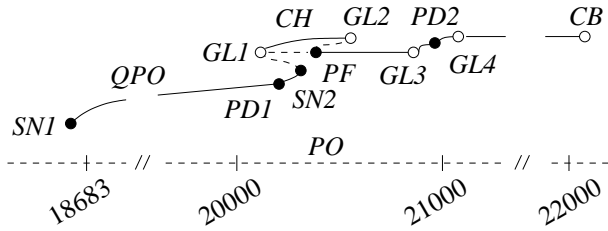
Figure 10: Schematic bifurcation diagram illustrating the sequence of bifurcations of tori leading to chaotic-drifting behaviour. Solid and dashed lines mean stable and unstable solutions, respectively. The labels PO and QPO indicate periodic and quasi-periodic orbits. The points SN, PF, PD and GL mean, respectively, saddle-node, pitchfork, period-doubling and gluing bifurcations, and CB chaotic-drifting behaviour. Local (PF, PD, SN) and global (GL, CB) bifurcations are indicated with closed and open circles, respectively. CH indicates the temporal chaotic solutions.
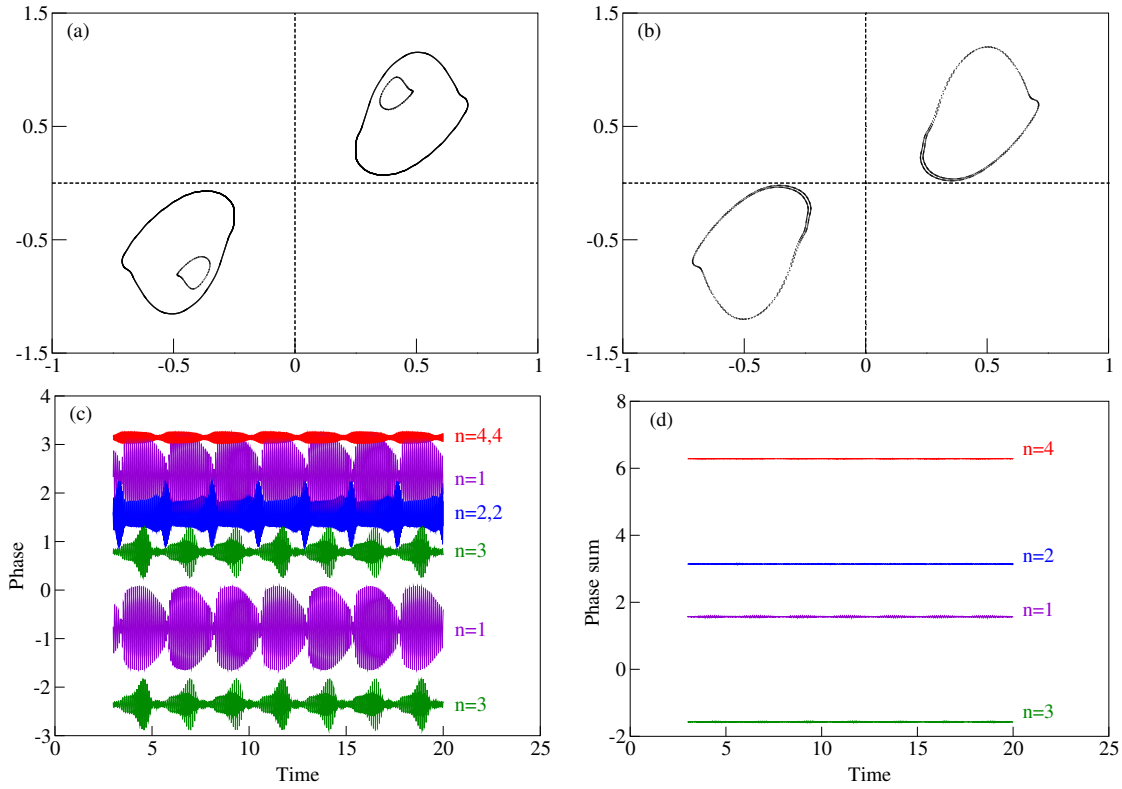
Figure 11: (a) Projections of the Poincaré section of two pairs of stable R_π-conjugate tori at Rayleigh numbers $Ra = 18500$ and $Ra = 20000$. They display the real part of the azimuthal Fourier coefficients $n = 3$ of v versus the $n = 1$ of u, both at a fixed radial point. (b) The same projection for a pair with double long period at $Ra = 20160$. (c) Phases of the $n = 1, .., 4$ Fourier coefficients of v of two conjugated tori versus time. (d) Sum of the phases of the Fourier coefficients with same n.
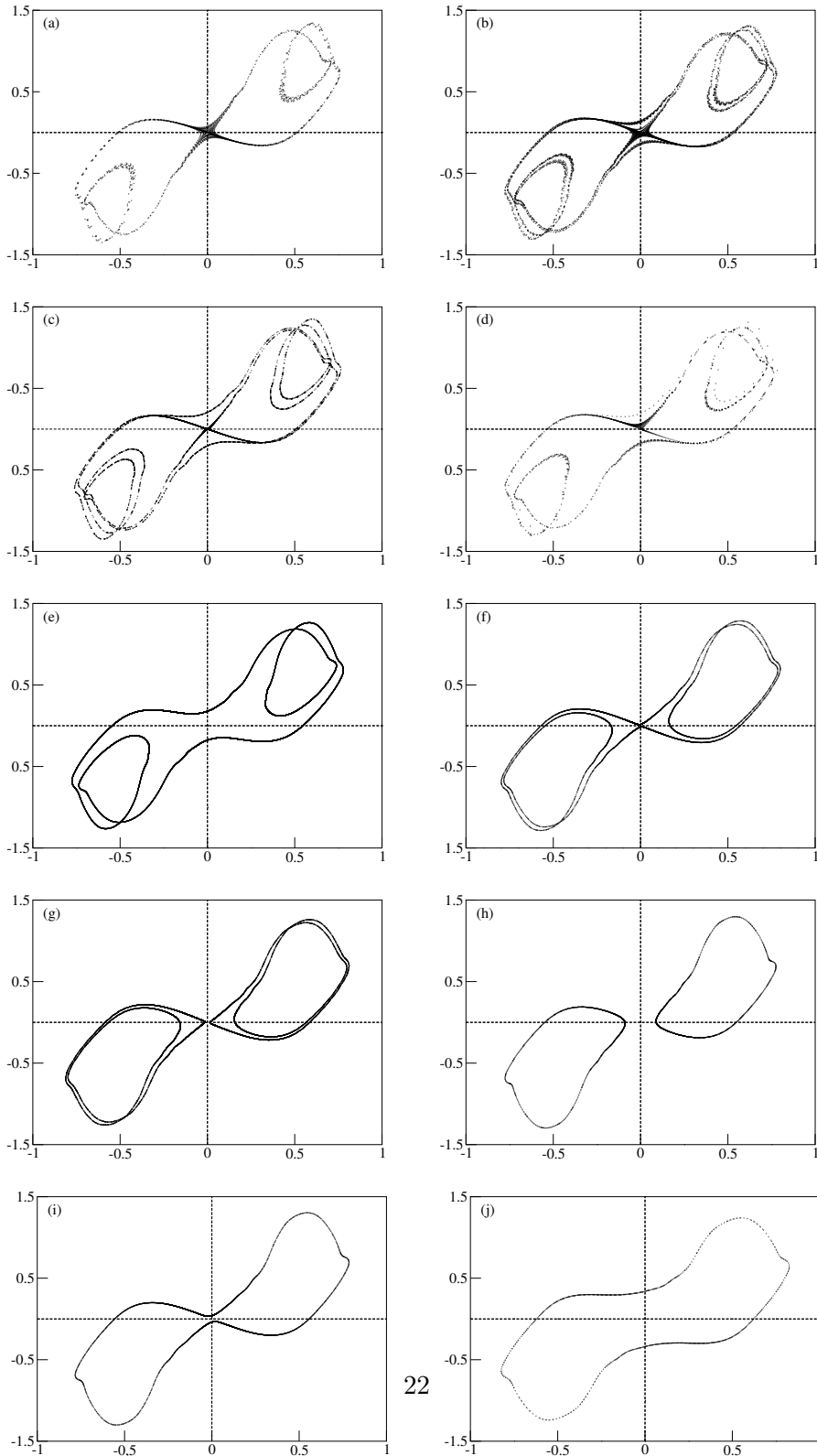
21

Figure 12: Poincaré sections of small and big tori showing the sequence of gluing bifurcations leading to *figure-of-eight* temporal chaotic attractors. The Rayleigh numbers are (a) 20120, (b) 20200, (c) 20240, (d) 20230, (e) 20500, (f) 20880, (g) 20910, (h) 20980 (i) 21020, (j) 22000.
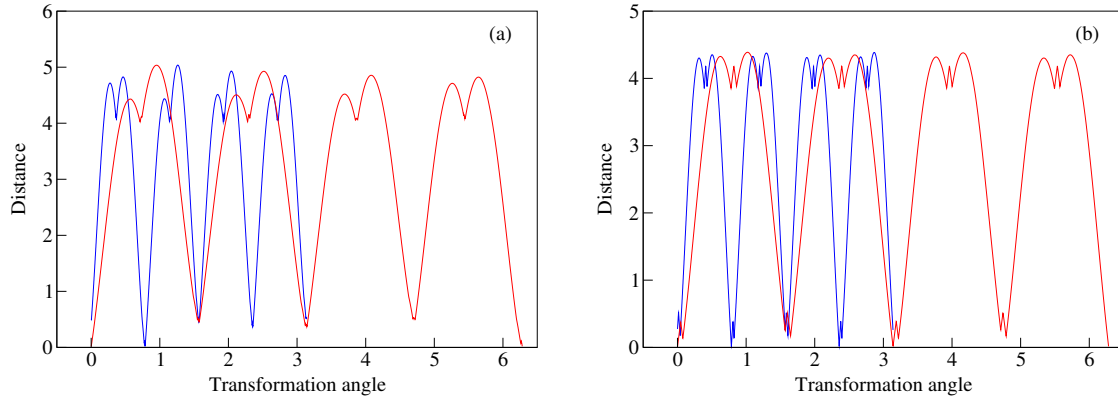
Figure 13: Distance d versus the angle of transformation, θ, for (a) a small torus at $Ra = 20000$, and (b) a big torus at $Ra = 20500$. Rotations and reflections are plotted in red and blue lines respectively.
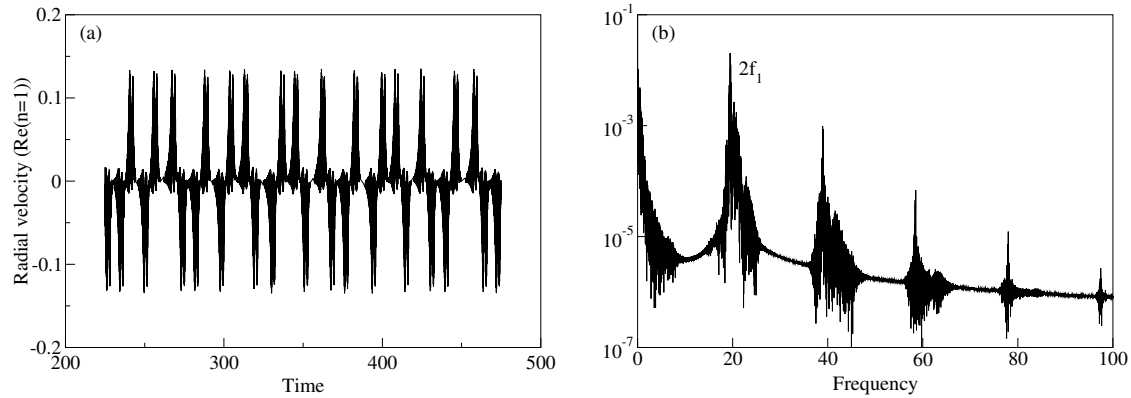

Figure 14: (a) Time series of the real part of the $n = 1$ Fourier coefficient of u at a fixed radial point. Each peak of the temporal series means a loop around the $n = 1$ DRTW. (b) Fourier spectrum of the Nusselt number defined in [Net *et al.*, 2003], for a chaotic attractor at $Ra = 20200$.

23
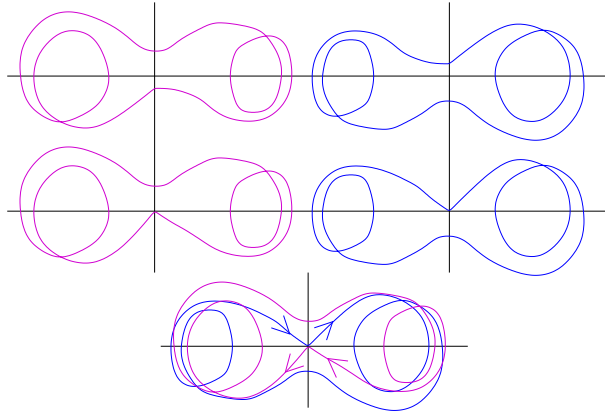
Figure 15: Sketch of the homoclinic connection on the unstable branch of the big asymmetric double-lobed tori.
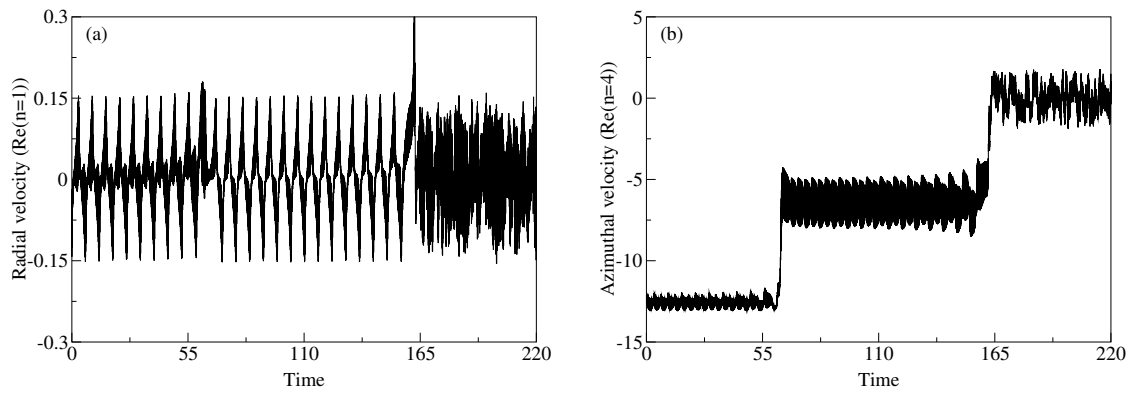
Figure 16: Time series at a fixed radial point of (a) the real part of the $n = 1$ Fourier coefficient of u, and (b) the real part of the $n = 4$ Fourier coefficient of v. $Ra = 22410$.

Figure 17: Time series at a fixed radial point of (a) the real part of the $n = 1$ Fourier coefficient of u, and (b) the real part of the $n = 4$ Fourier coefficient of v. (c) Detail of (b) displaying the fast excursions among R_α-conjugate tori at $Ra = 27000$. (d) Tridimensional phase map showing the group orbit of the $n = 4$ DRTW (red line), and a chaotic-drifting orbit (blue line).

25

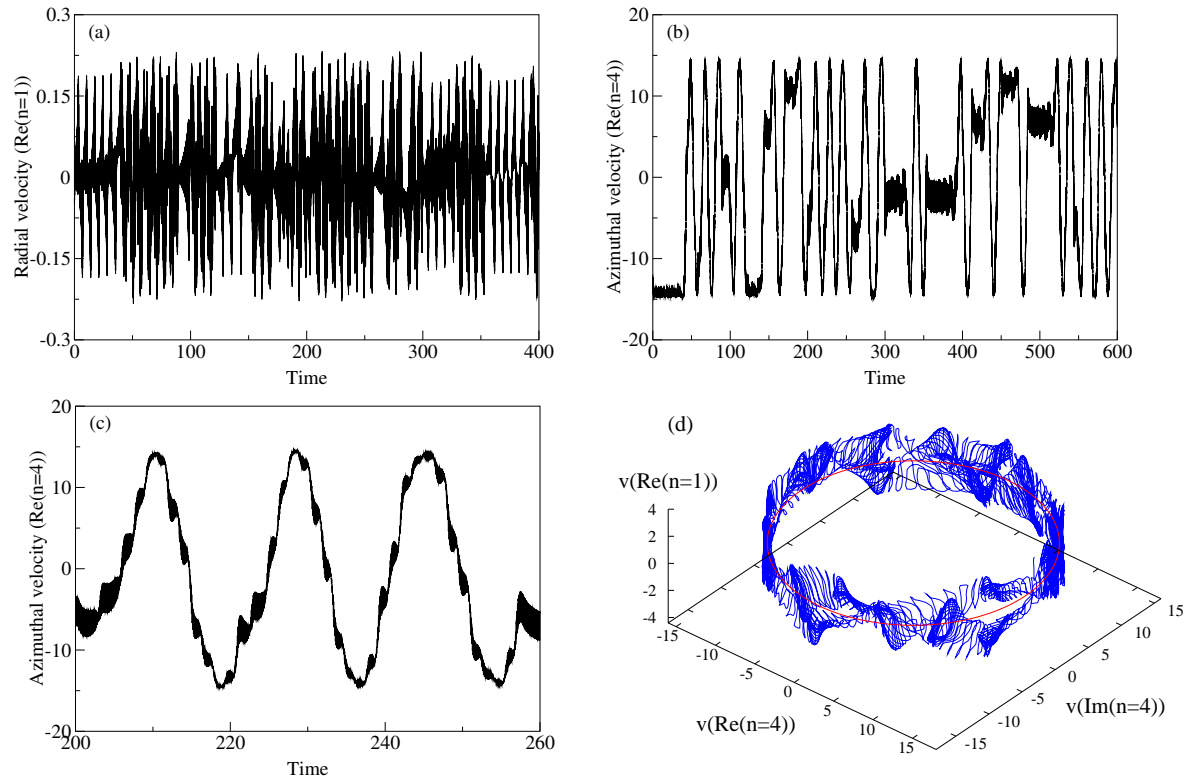Table 1: Evolution of the first five FM on the $n = 4$ branch of Fig. 1. The marginal $\mu = 1$ FM due to the invariance of the system by rotation is not tabulated.

Ra	μ_1	μ_2	μ_3	μ_4	μ_5
10100	0.99894	0.94876+0.11459i	0.94876-0.11459i	0.94876+0.11459i	0.94876-0.11459i
10300	1.00084	0.94972+0.11241i	0.94972-0.11241i	0.94972+0.11241i	0.94972-0.11241i
11300	1.00829	0.95315+0.09829i	0.95315-0.09829i	0.95315+0.09829i	0.95315-0.09829i
12300	1.01234	0.95471+0.07854i	0.95471-0.07854i	0.95471+0.07854i	0.95471-0.07854i
13300	1.01300	0.95503+0.05017i	0.95503-0.05017i	0.95503+0.05017i	0.95503-0.05017i
14000	1.01148	0.95492+0.00789i	0.95492-0.00789i	0.95490+0.00780i	0.95490-0.00780i
14300	1.01033	0.98535	0.98535	0.94073	0.92451
14600	1.00891	0.99803	0.99803	0.94102	0.91189
14660	1.00856	1.00000	1.00000	0.94108	0.90980
14700	1.00837	1.00132	1.00132	0.94112	0.90856
15100	1.01216	1.01216	1.00592	0.94149	0.89815
15800	1.02529	1.02529	1.00057	0.94209	0.88669
15900	1.02677	1.02677	0.99970	0.94217	0.88559
16900	1.03730	1.03730	0.98996	0.94291	0.87915
17900	1.04247	1.04247	0.97907	0.94355	0.87796
18900	1.04414	1.04414	0.96831	0.94408	0.87818
20000	1.04352	1.04352	0.95788	0.94457	0.87730
20060	1.04344	1.04344	0.95737	0.94460	0.87718
20150	1.04331	1.04331	0.95661	0.94463	0.87699
20200	1.04323	1.04323	0.95619	0.94465	0.87687
20250	1.04315	1.04315	0.95578	0.94467	0.87675
20850	1.04204	1.04204	0.95116	0.94489	0.87479
20900	1.04194	1.04194	0.95080	0.94491	0.87459
20950	1.04183	1.04183	0.95045	0.94493	0.87438
21000	1.04172	1.04172	0.95010	0.94494	0.87416
21030	1.04166	1.04166	0.94989	0.94495	0.87403
21510	1.04054	1.04054	0.94671	0.94511	0.87180
21750	1.03993	1.03993	0.94523	0.94518	0.87013
21790	1.03982	1.03982	0.94519	0.94499	0.86987
21990	1.03929	1.03929	0.94525	0.94381	0.86854
22300	1.03843	1.03843	0.94533	0.94208	0.86630
22350	1.03829	1.03829	0.94534	0.94181	0.86592
22520	1.03780	1.03780	0.94539	0.94090	0.86459
22920	1.03660	1.03660	0.94548	0.93886	0.86123
23320	1.03534	1.03534	0.94556	0.93693	0.85758
23920	1.03335	1.03335	0.94568	0.93422	0.85163
24500	1.03133	1.03133	0.94577	0.93176	0.84542

Table 2: Evolution of the first five FM on the $n = 1$ branch that starts at $Ra = 17497$ in Fig. 1. The marginal $\mu = 1$ FM due to the invariance of the system by rotation is not tabulated.

Ra	μ_1	μ_2	μ_3	μ_4	μ_5
17480	1.15244	0.99919	0.94891	0.91565	0.88025+0.21271i
17550	1.14243	0.99467	0.94821	0.87802+0.21433i	0.87802-0.21433i
18240	1.11183	0.98425	0.81693+0.50851i	0.81693-0.50851i	0.94870
18500	1.10439	0.82949+0.53328i	0.82949-0.53328i	0.98211	0.94889
18700	1.09919	0.83767+0.54846i	0.83767-0.54846i	0.98045	0.94902
19260	1.08677	0.85616+0.58034i	0.85616-0.58034i	0.97489	0.94936
19980	1.07522	0.87379+0.60971i	0.87379-0.60971i	0.96626	0.94984
20060	1.07420	0.87547+0.61260i	0.87547-0.61260i	0.96532	0.94989
20160	1.07298	0.87750+0.61613i	0.87750-0.61613i	0.96417	0.94996
20180	0.87790+0.61683i	0.87790-0.61683i	1.07274	0.96394	0.94997
20240	0.87908+0.61891i	0.87908-0.61891i	1.07205	0.96327	0.95002
20400	0.88215+0.62437i	0.88215-0.62437i	1.07029	0.96158	0.95013
20580	0.88548+0.63038i	0.88548-0.63038i	1.06844	0.95982	0.95025
20820	0.88979+0.63817i	0.88979-0.63817i	1.06611	0.95777	0.95042
20980	0.89263+0.64323i	0.89263-0.64323i	1.06460	0.95657	0.95054
21060	0.89404+0.64571i	0.89404-0.64571i	1.06384	0.95602	0.95059
21200	0.89653+0.64998i	0.89653-0.64998i	1.06249	0.95512	0.95069
21700	0.90554+0.66411i	0.90554-0.66411i	1.05703	0.95256	0.95107
22000	0.91100+0.67161i	0.91100-0.67161i	1.05284	0.95162	0.95132
22200	0.91453+0.67618i	0.91453-0.67618i	1.04948	0.95151	0.95143
22300	0.91624+0.67835i	0.91624-0.67835i	1.04758	0.95161	0.95153
22400	0.91788+0.68046i	0.91788-0.68046i	1.04552	0.95179	0.95172
22500	0.91945+0.68251i	0.91945-0.68251i	1.04328	0.95223	0.95184
22700	0.92229+0.68652i	0.92229-0.68652i	1.03816	0.95371	0.95212
23000	0.92560+0.69258i	0.92560-0.69258i	1.02850	0.95752	0.95269
23400	0.92781+0.70161i	0.92781-0.70161i	1.01000	0.96425	0.95416
23600	0.92834+0.70671i	0.92834-0.70671i	0.99692	0.96673	0.95579
23800	0.92936+0.71181i	0.92936-0.71181i	0.97912	0.96724	0.96006
23900	0.93034+0.71413i	0.93034-0.71413i	0.96666	0.96587+0.00701i	0.96587-0.00701i
24100	0.93343+0.71787i	0.93343-0.71787i	0.96449	0.95809+0.01553i	0.95809-0.01553i
24500	0.94257+0.72038i	0.94257-0.72038i	0.96524	0.94352+0.01394i	0.94352-0.01394i